

Improve Transmission Fault Location and Distance Protection Using Accurate Line Parameters

Hugo E. Prado-Félix and Víctor H. Serna-Reyna, *Comisión Federal de Electricidad*
Mangapathirao V. Mynam, Marcos Donolo, and Armando Guzmán, *Schweitzer Engineering Laboratories, Inc.*

Abstract—Accurate positive- and zero-sequence line impedances are critical for the performance of distance relaying and fault location. This paper discusses a method for calculating positive- and zero-sequence line impedances under single-pole open conditions. Time-synchronized measurements from both terminals of the line are captured when one pole of either terminal is open. This operational condition provides an unbalance in the three-phase network, which is used to measure the line impedances. The performance of the method has been verified using Electromagnetic Transients Program (EMTP) simulations and field data provided by Comisión Federal de Electricidad (CFE). The paper also discusses existing methods to calculate line parameters and provides a sensitivity analysis of these methods. The paper presents an approach where the calculated impedances can be compared with the relay impedance settings and an alarm sent if the difference is greater than a predetermined threshold.

I. INTRODUCTION

Accurate transmission line parameters are critical for many impedance-based applications, including distance protection and fault location. Line parameters are typically calculated based on tower configuration and conductor physical properties. Several factors affect the accuracy of the calculations, including temperature and ground resistivity. Some utilities conduct field tests to measure the parameters of transmission lines. The test process includes an outage of the line. The line is shorted to ground at the remote end and energized with a known source at the local end. References [1] and [2] use time-synchronized voltage and current measurements from both terminals of the transmission line to measure the impedance during normal operating conditions.

Section II of this paper discusses the errors in line parameters and their effect on distance protection and fault location. Section III discusses classical methods for determining positive- and zero-sequence line impedances. Section IV discusses a method to estimate the line parameters during normal and single-pole open (SPO) operating conditions using time-synchronized measurements. Section V discusses the validation of the SPO-based method using Electromagnetic Transients Program (EMTP) simulations, and Section VI uses field data from a Comisión Federal de Electricidad (CFE) 400 kV network to estimate line parameters. Section VII discusses a proposal to monitor the line impedances during SPO conditions and send an alarm when the estimated impedance and the relay settings differ significantly.

II. ERRORS IN LINE PARAMETERS AND THEIR EFFECT ON DISTANCE PROTECTION AND FAULT LOCATION

To show how errors in transmission line parameters affect distance element and fault locating accuracy, we first review the equations used by these algorithms. Then we show the worst-case estimates of the distance to the fault that include impedance setting errors for a given fault condition.

A. Distance Protection

Distance-based line protection uses positive- and zero-sequence impedances along with voltage and current measurements to determine if faults are inside the protection zone. One method to estimate the distance to the fault for A-phase-to-ground faults by mho elements is provided in (1).

$$mAG = \frac{\text{Real}(V_a \cdot V_{pol}^*)}{\text{Real}(Z_{1L} \cdot (I_a + k_0 \cdot I_G) \cdot V_{pol}^*)} \quad (1)$$

where:

V_a is the faulted phase voltage.

V_{pol} is the polarizing quantity.

I_a is the faulted phase current.

I_G is the residual current.

Z_{0L} is the zero-sequence line impedance.

Z_{1L} is the positive-sequence line impedance.

k_0 is the zero-sequence compensation factor $\frac{Z_{0L} - Z_{1L}}{3Z_{1L}}$.

If the computed value mAG is less than the relay reach setting, the relay declares an in-zone fault.

B. Single-Ended Fault Location

This fault location method uses local voltages and currents. Equation (2) shows the fault location equation for an A-phase-to-ground fault.

$$FL_{AG_{SE}} = \frac{\text{Imag}(V_a \cdot I_2^*)}{\text{Imag}(Z_{1L} \cdot (I_a + k_0 \cdot I_G) \cdot I_2^*)} \quad (2)$$

where:

I_2 is the negative-sequence current.

The accuracy of the fault location depends on the accuracy of the line parameter settings, fault resistance, system nonhomogeneity, and zero-sequence mutual impedance (if mutually coupled lines are present).

C. Multi-Ended Fault Location Using Remote Terminal Currents

This fault location method uses voltages and currents from the local terminal of the line along with currents from the remote terminal(s). Equation (3) shows the fault location equation for A-phase-to-ground faults [3].

$$FL_AG_{MEI} = \frac{\text{Imag}(V_a \cdot I_{2T}^*)}{\text{Imag}(Z_{1L}(I_a + k_0 \cdot I_G) \cdot I_{2T}^*)} \quad (3)$$

where:

I_{2T} is the sum of the local and remote negative-sequence currents.

This method is typically used in line differential relays, which have access to remote currents for differential protection purposes. The accuracy of this method is not influenced by system nonhomogeneity and fault resistance; however, errors in zero- and positive-sequence line impedances influence the accuracy of the fault location. If mutually coupled lines are present, zero-sequence mutual impedance also affects the accuracy of the estimation.

D. Multi-Ended Fault Location Using Remote Terminal Currents and Voltages

This fault location method uses voltages and currents from the local and remote terminals [4] [5]. It uses (4) to obtain the fault location for unbalanced faults.

$$FL_UNB_{ME} = \text{Real}\left(\frac{V_{2L} - V_{2R} + I_{2R} \cdot Z_{1L}}{I_{2T} \cdot Z_{1L}}\right) \quad (4)$$

where:

V_{2L} is the negative-sequence voltage at the local terminal.

V_{2R} and I_{2R} are the negative-sequence voltage and current at the remote terminal, respectively.

This method can be used in line differential relays, which have access to remote currents and voltages. The accuracy of this method is not influenced by the system homogeneity and fault resistance. A key benefit of this method is that it is independent of Z_{0L} . Therefore, the actual fault location reported by the line crew provides feedback on the accuracy of positive-sequence line impedance.

E. Distance to Fault Estimation Errors

We use (1) to study the effect of line parameter errors on the distance to the fault. We represent the relay setting Z_{1L} as follows:

$$Z_{1L} = Z_1 + \varepsilon_{Z1} \quad (5)$$

where:

Z_1 is the actual positive-sequence impedance value.

ε_{Z1} is the error.

To obtain the expression for Z_{0L} , we replace 1 with 0 in (5). Fig. 1 shows the actual impedance Z_1 and the relay setting Z_{1L} with an error with fixed magnitude and variable phase angle.

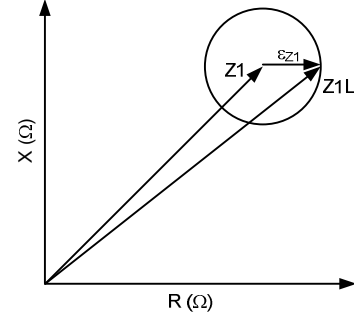


Fig. 1. Relay setting represented as the sum of the actual impedance and setting error.

Using (1) with Z_{1L} and Z_{0L} settings, ε_{Z1} equal to 3 percent, ε_{Z0} equal to 10 percent, and simulation results for an A-phase-to-ground fault with zero fault resistance at 80 percent of the line (see the appendix for the system details), we find the minimum value of m to be 0.73 of the line length. Proceeding in the same way, we obtain a maximum value of m of 0.86 of the line length. Fig. 2 shows the minimum values of m for all the combinations of errors in Z_{0L} and Z_{1L} between 0 and 25 percent. Fig. 3 shows the maximum values of m for all the combinations of errors in Z_{0L} and Z_{1L} between 0 and 25 percent.

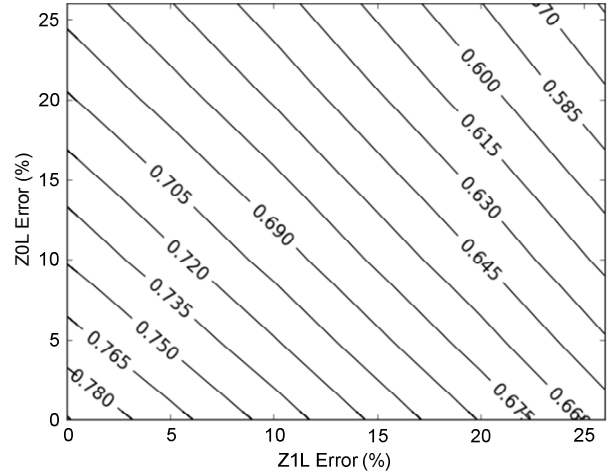


Fig. 2. Minimum values of m as a function of the error in Z_{1L} and Z_{0L} for a fault at 80 percent of the line.

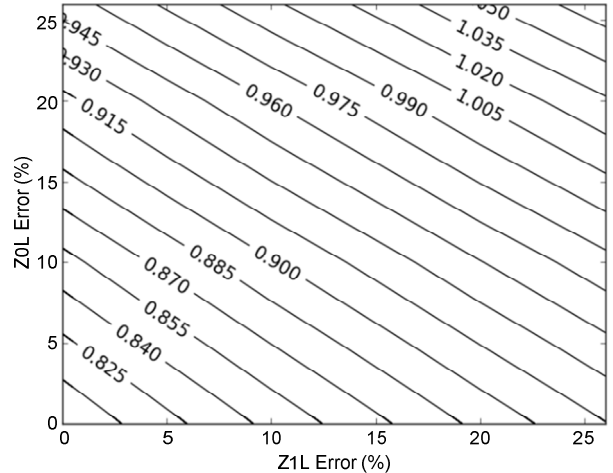


Fig. 3. Maximum values of m as a function of the error in Z_{1L} and Z_{0L} for a fault at 80 percent of the line.

These values are true for the mho element m calculation, the single-ended fault location method, and the multi-ended fault location method that uses remote currents only.

The multi-ended fault location method that uses voltages and currents from the remote terminal does not depend on Z0L. Typically, Z0L has greater errors than Z1L; therefore, this method provides more accurate distance-to-fault estimates than the other methods. Fig. 4 shows the effect of errors in Z1L on the fault location estimation of this method.

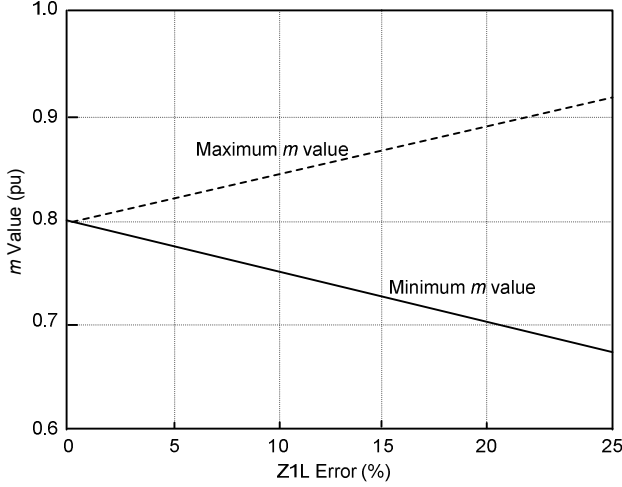


Fig. 4. Maximum and minimum m values due to errors in Z1L for the multi-ended fault location method.

III. METHODS TO DETERMINE LINE PARAMETERS

Existing methods to determine the line parameters can be categorized as follows:

- Parameter calculations using line constants programs.
- Parameter measurements using signal injection equipment.
- Parameter estimation using time-synchronized measurements (this method is discussed in Section IV).

A. Line Constants Programs

Typically, line parameters are computed using line constants programs, which are widely available. These programs use tower configuration and conductor properties to calculate the parameters. Ground resistivity is one of the variables that is difficult to determine. Ground resistivity, which affects the resistance of the return path for the fault current back to the substation ground, depends on the terrain and weather. References [6] and [7] discuss the impact of ground resistivity on the estimation of the zero-sequence line impedance. Fig. 5 shows the effect of ground resistivity on the zero-sequence impedance of a typical 400 kV line.

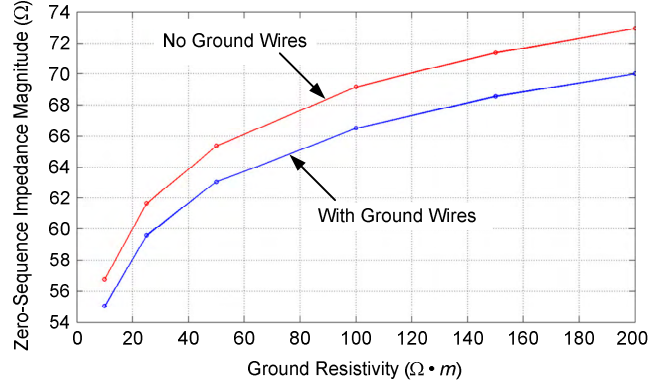


Fig. 5. Effect of ground resistivity on zero-sequence impedance.

B. Signal Injection Methods for Measuring Line Parameters

Signal injection is an option that utilities have to measure line parameters; it requires a line outage and an adequate power source.

The following procedure was used at CFE to determine the parameters of lines where distance protection schemes showed overreach problems.

As Fig. 6 shows, all three phases and ground conductors (if present) are shorted and connected to ground at one end of the transmission line.

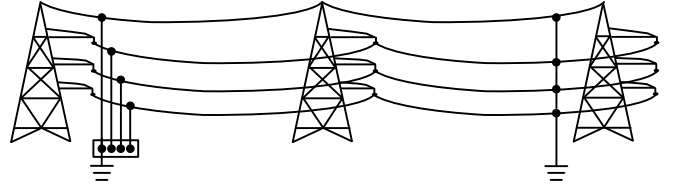


Fig. 6. Test setup to measure the line parameters.

At the other end of the transmission line, signals are injected and voltage and current measurements are taken to determine the line impedances. This method requires three phase-to-phase impedance measurements (Z_{ab} , Z_{bc} , and Z_{ca}), along with three phase-to-ground impedance measurements (Z_{ag} , Z_{bg} , and Z_{cg}) and a zero-sequence impedance measurement (Z_{0g}) [8].

Positive-sequence impedance (Z_{1m}) is computed from the measurements using (6).

$$Z_{1m} = \frac{\frac{1}{2}(Z_{ab} + Z_{bc} + Z_{ca})}{3} \quad (6)$$

Zero-sequence impedance (Z_{0m}) is computed using (7) and (8).

$$Z_e = \frac{Z_{ag} + Z_{bg} + Z_{cg}}{3} - Z_{1m} \quad (7)$$

$$Z_{0m} = \frac{(Z_{1m} + 3Z_e) + 3Z_{0g}}{2} \quad (8)$$

It is important to note that these measurements do not include errors in voltage transformers (VTs) and current transformers (CTs) that still affect the performance of the distance protection and fault location schemes.

IV. ESTIMATING LINE PARAMETERS USING TIME-SYNCHRONIZED MEASUREMENTS

Time-synchronized measurements are available as synchrophasors and as time-synchronized samples of instantaneous signals. Time-synchronized sampling is the mechanism where the data acquisition in protective relays or digital fault recorders (DFRs) acquires voltage or current samples with respect to an absolute time reference, typically Global Positioning System (GPS). Synchronized measurements allow us to perform mathematical operations on quantities measured at different locations in the power system, in this case, measurements from both terminals of the line.

A. PI Model Approach

A common approach to measure positive-sequence line impedance uses a PI equivalent model of the transmission line [9]. Fig. 7 shows the positive-sequence PI equivalent of the line, and (9) estimates the positive-sequence impedance.

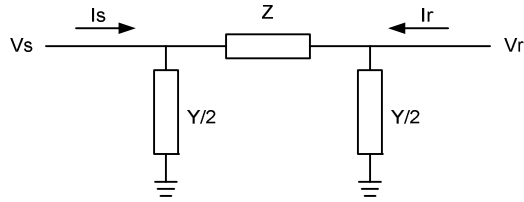
$$Z = R + jX = \frac{V_s^2 - V_r^2}{I_s \cdot V_r - I_r \cdot V_s} \quad (9)$$


Fig. 7. PI equivalent model of the transmission line.

The load angle δ between V_s and V_r and the CT and VT errors have an important effect on the quality of the impedance estimation in (9). Fig. 8 shows that for small phase angle differences between V_s and V_r (load angle δ less than 5 degrees), small CT and VT errors are greatly amplified. Fig. 8 also shows that CT and VT accuracies have a great impact on the impedance estimation.

For angles δ greater than 5 degrees, the calculation error decreases rapidly. We show an example of this problem in Section V, Subsection B.

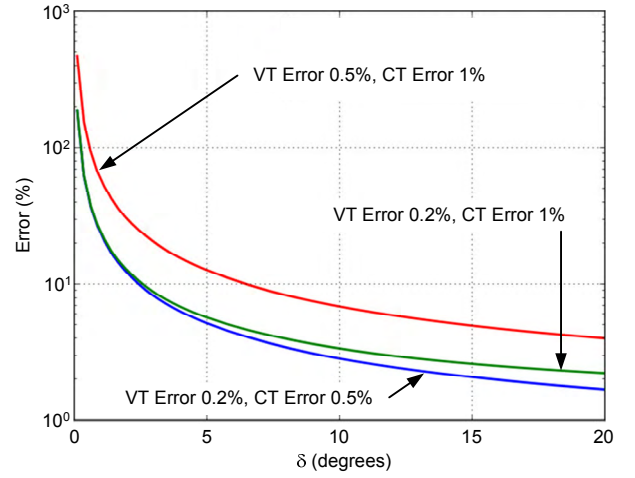


Fig. 8. Estimation error as a function of the angle between V_s and V_r for three different CT and VT error ratings for the PI model approach.

B. Single-Pole Open Method

The method discussed in the previous subsection provides an estimate of the positive-sequence impedance only. Unbalanced system conditions are required to calculate the zero-sequence impedance. Reference [7] discusses calculating the positive- and zero-sequence impedances during ground faults; this approach requires the actual fault location and the fault voltages and currents at both terminals to calculate the positive- and zero-sequence impedances. Traveling wave fault location devices are used for providing accurate fault location within a tower span. Therefore, fault location results from the traveling wave approach along with the voltages and currents from both terminals of the transmission line can be used to compute line parameters.

Here, we propose calculating the positive- and zero-sequence impedances of the line while one pole is open at only one end of the line. Fig. 9 shows a two-terminal system with A-phase open at Terminal X.

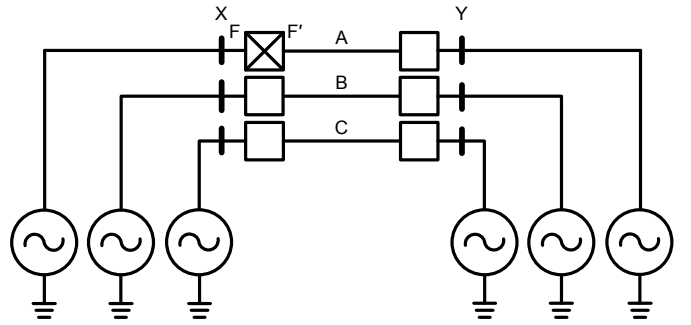


Fig. 9. Two-terminal system with SPO condition.

This method can be used on transmission systems with single-pole breaker control mechanisms and line-side VTs [10] [11]. Fig. 10 shows the sequence network for the line shown in Fig. 9. As we know, the positive- and negative-sequence line impedances of transmission lines are the same. We selected the negative-sequence network to calculate the negative-sequence impedance because the effect of charging current on the calculation method is lower in the negative-sequence network than in the positive-sequence network when the phase is open at only one end.

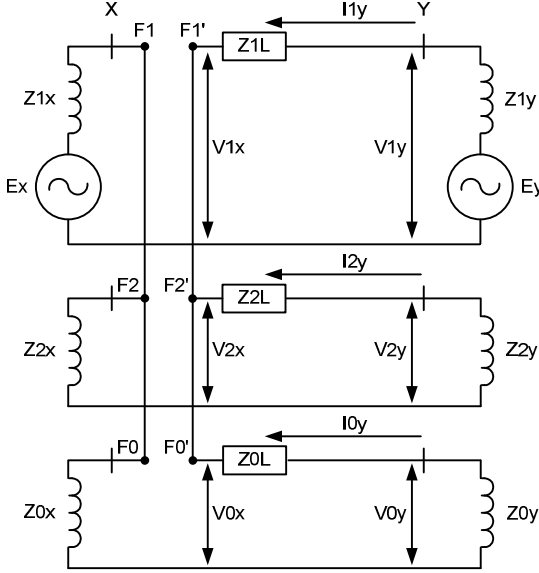


Fig. 10. Symmetrical component network representation of an SPO condition at Terminal X.

Equations (10) and (11) show the positive-, negative-, and zero-sequence impedance calculations.

$$Z1L = (V2y - V2x) / I2y = Z2L \quad (10)$$

$$Z0L = (V0y - V0x) / I0y \quad (11)$$

where:

$V2x$ is the negative-sequence voltage calculated at Terminal X.

$V2y$ is the negative-sequence voltage calculated at Terminal Y.

$I2y$ is the negative-sequence current calculated at Terminal Y.

$V0x$ is the zero-sequence voltage calculated at Terminal X.

$V0y$ is the zero-sequence voltage calculated at Terminal Y.

$I0y$ is the zero-sequence current calculated at Terminal Y.

The SPO method depends on the negative-sequence voltage difference between the two terminals for the negative-sequence impedance estimation and on the zero-sequence voltage difference for the zero-sequence impedance estimation.

As with the PI model approach, the load angle δ and the CT and VT errors have an important effect on the quality of the impedance estimation in (10) and (11). Fig. 11 shows the positive-sequence impedance calculation error, computed with (10) for the SPO method as a function of the CT and VT errors and the load angle.

This method is not recommended for lightly loaded conditions. The zero-sequence mutual impedance in mutually coupled line configurations affects the estimation of zero-sequence line impedance using the SPO method.

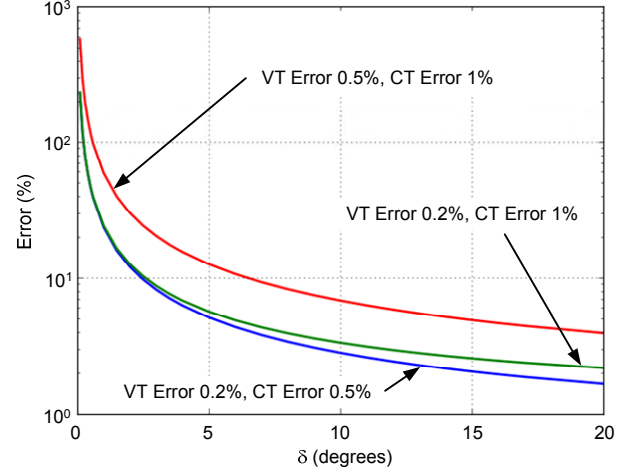


Fig. 11. Estimation error in the positive-sequence line impedance as a function of the load angle δ for two different CT and VT error ratings for the SPO method.

V. EMTP SIMULATION RESULTS

We modeled a two-source one-line system to verify the performance of the SPO method. The modeled 252-kilometer transposed line is part of the CFE 400 kV transmission network between the MZD and TPD substations. Fig. 12 shows the one-line diagram with relays connected to both terminals.

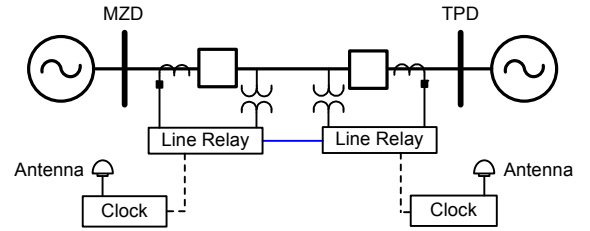


Fig. 12. Test system with line relays connected to GPS.

The power system was modeled in a Real Time Digital Simulator[®], which runs EMTP, along with CTs and coupling capacitor voltage transformers (CCVTs). The outputs of the CTs and CCVTs are connected to the relays protecting the 252-kilometer transmission line. The relays at both terminals are configured to trigger event reports when line faults occur. Additionally, both relays are configured to stream synchrophasor data to a phasor data concentrator with archiving capability.

A. SPO Method Using Time-Synchronized Instantaneous Samples

An A-phase-to-ground fault was simulated at 242 kilometers from the MZD terminal. Fig. 13 shows the time-aligned event reports from the MZD and TPD terminals. The relay at TPD detected the fault and tripped the breaker half a cycle earlier than the relay at MZD.

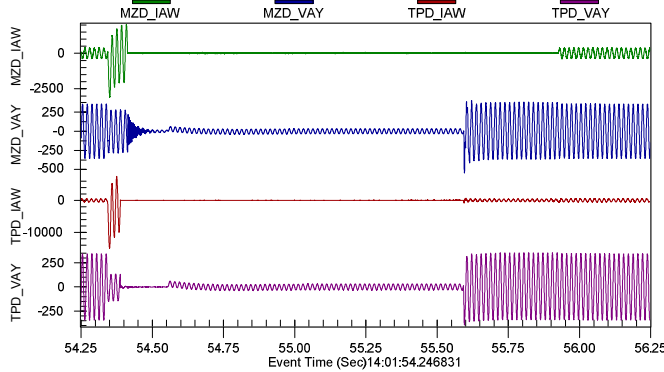


Fig. 13. Faulted phase voltages and currents at both terminals for a fault at 242 kilometers from MZD.

For this fault, the TPD terminal recloses prior to the MZD terminal after the 1.2-second open-interval timer expires. The MZD terminal has an SPO condition with the TPD terminal closed. Voltages and currents from both terminals in this period of an SPO condition are used for computation of the positive- and zero-sequence line impedances. Data are post-processed to compute the positive- and zero-sequence line impedances. Fig. 14 shows the signal processing flow.

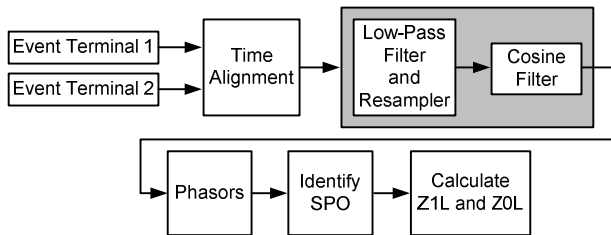


Fig. 14. Signal processing to compute Z_{1L} and Z_{0L} .

Event reports are retrieved from both terminals and time-aligned to adjust for different trigger times. If the event reports are based on a fixed sampling rate (samples per second), the aligned data are processed using a low-pass filter and resampled to 32 samples per cycle. A cosine filter is then used to extract the fundamental quantity of the signal and filter out dc and harmonics. Processing in the highlighted section of Fig. 14 is not required when using filtered event reports. The cosine-filtered signal is then used to construct the phasors.

We use the logic shown in Fig. 15 to identify local SPO conditions while the remote terminal is closed.

Equations (10) and (11) are used to calculate the line impedances based on the data corresponding to this condition. Fig. 16 shows the comparison of the estimated positive-sequence impedance during the SPO condition with the line

impedance calculated by the line constants calculation (LCC) program. Fig. 17 shows the same comparison for zero-sequence impedance.

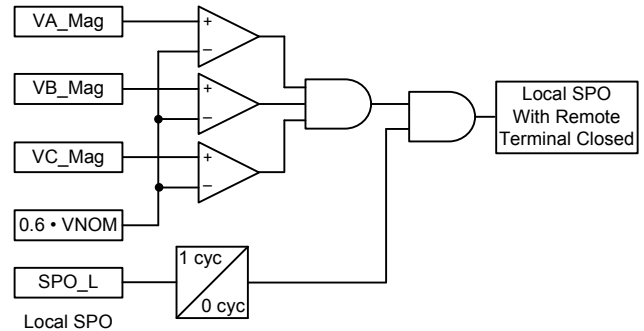


Fig. 15. Logic to detect SPO condition with the remote terminal closed.

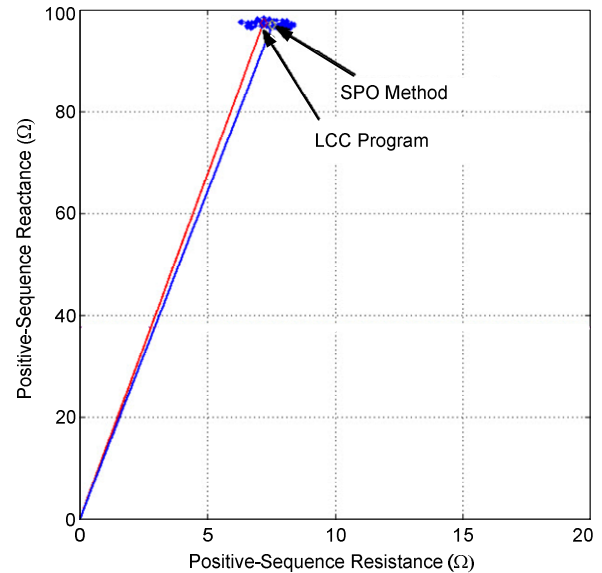


Fig. 16. Positive-sequence line impedance comparison between the LCC program and SPO method.

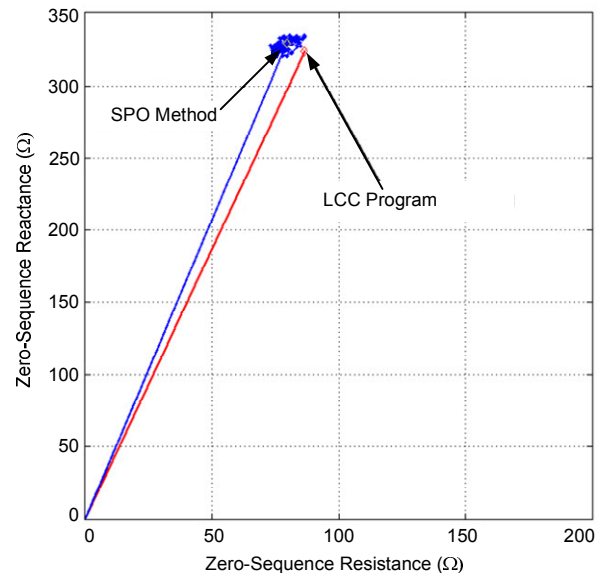


Fig. 17. Zero-sequence line impedance comparison between the LCC program and SPO method.

Fig. 18 shows the real-time zero-sequence resistance and reactance calculations (implemented using relay programmable logic) performed by the relay at the MZD terminal using time-synchronized local and remote voltages and currents [12].

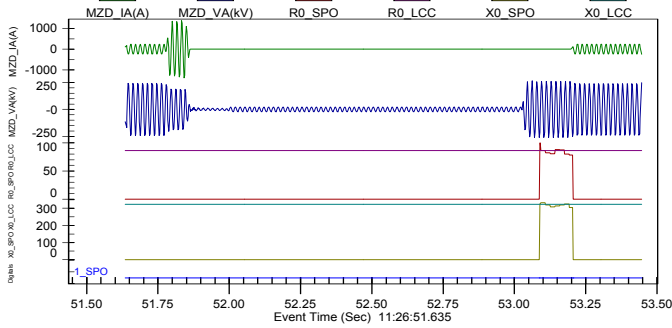


Fig. 18. Real-time zero-sequence impedance calculations.

Table I shows the average line impedance results estimated during SPO conditions using time-synchronized samples.

TABLE I
LINE IMPEDANCES ESTIMATED WITH THE LCC PROGRAM AND DURING SPO CONDITIONS USING TIME-SYNCHRONIZED SAMPLES

| Method | Positive Sequence (primary ohms) | Zero Sequence (primary ohms) |
|-------------|----------------------------------|------------------------------|
| LCC program | $7.2 + j \cdot 97.32$ | $86.52 + j \cdot 323.4$ |
| SPO | $8.16 + j \cdot 97.27$ | $80.59 + j \cdot 323.3$ |

B. Synchrophasor-Based SPO Method

Synchrophasor measurements were archived during the simulation. Fig. 19 shows the faulted phase current and voltage magnitudes, during pre-fault, fault, and post-fault.

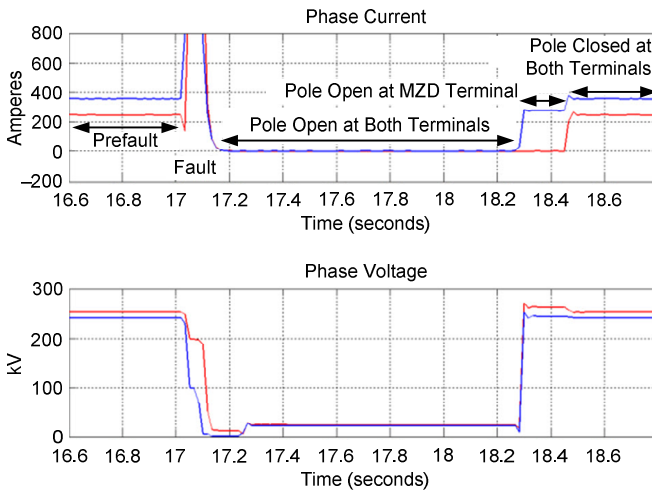


Fig. 19. Synchrophasor measurements from both terminals for a trip and reclose sequence (MZD is shown by the red trace; TPD by the blue).

Table II shows the line impedance calculated during the normal load conditions using the PI model approach and during the SPO condition using synchrophasors in primary ohms.

TABLE II
LINE IMPEDANCES ESTIMATED USING SYNCHROPHASOR MEASUREMENTS

| Method | Positive Sequence (primary ohms) | Zero Sequence (primary ohms) |
|----------|----------------------------------|------------------------------|
| PI model | $6.96 + j \cdot 95.59$ | NA |
| SPO | $5.96 + j \cdot 96.54$ | $86.11 + j \cdot 324.7$ |

VI. FIELD RESULTS

A. Signal Injection-Based Testing at CFE

We compared line parameters obtained using the signal injection method and the LCC program on four transmission lines.

1) GDU-CLN 6.5-Kilometer 230 kV Line

The first line we studied was the 6.5-kilometer 230 kV line from GDU to CLN, which is an underground cable. Fig. 20 shows the measured ($Z0m$ and $Z1m$) and computed ($Z0lcc$ and $Z1lcc$) values.

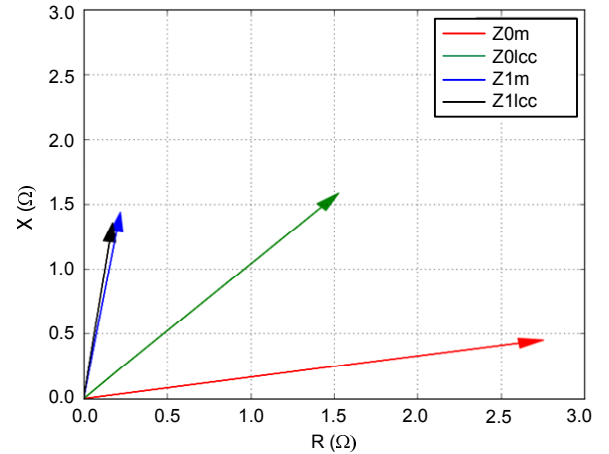


Fig. 20. Measured ($Z0m$ and $Z1m$) and computed ($Z0lcc$ and $Z1lcc$) values for a 6.5-kilometer 230 kV line. Note the disparity between $Z0m$ and $Z0lcc$.

If we use the measured impedances to compute currents and voltages for an A-phase-to-ground fault at 80 percent of the line length, a distance function using the impedance values from the LCC program will see the fault at 95 percent of the line.

2) GDU-SCU 14.8-Kilometer 69 kV Line

The second line we studied was the 14.8-kilometer 69 kV line from GDU to SCU, which is part underground cable and part overhead line. Fig. 21 shows the measured and computed positive- and zero-sequence impedance values.

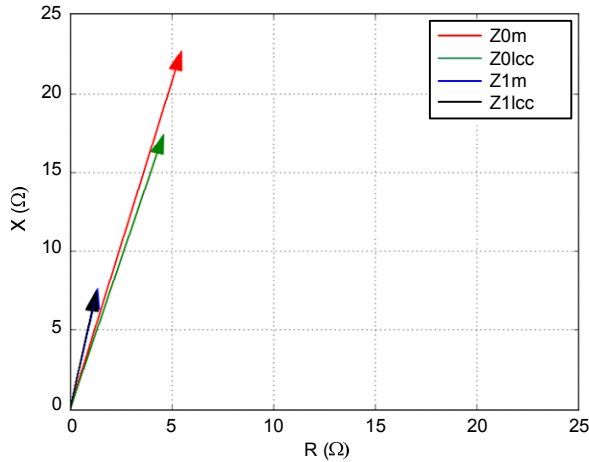


Fig. 21. Measured and computed positive- and zero-sequence impedances for a 14.8-kilometer 69 kV line.

In this case, the difference between the measured and the computed values of the line impedances causes a fault at 80 percent of the line to look like a fault at 67 percent, which causes the distance element to overreach.

3) APT-AGT 36-Kilometer 230 kV Line

The third line we studied was the 36-kilometer 230 kV line from APT to AGT, which is an overhead line. Fig. 22 shows the measured and computed positive- and zero-sequence impedance values.

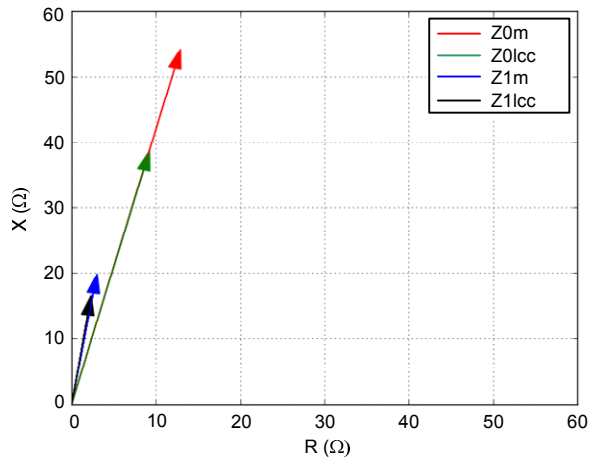


Fig. 22. Measured and computed positive- and zero-sequence impedance for a 36-kilometer 230 kV line. Note that while the X/R ratios are very accurate, there is a large difference in magnitude.

In this case, the differences between the measured and computed positive- and zero-sequence impedance values are significant. These differences cause a fault at 80 percent of the line to look like a fault at 59 percent, which implies that the relay will overreach by about 21 percent. In this case, CFE modified the relay settings according to the measurements.

4) AGS-AGN 5.4-Kilometer 115 kV Line

Finally, we studied the 5.4-kilometer 115 kV line between AGS and AGN, which is an overhead line. Fig. 23 shows the measured and computed positive- and zero-sequence impedance values.

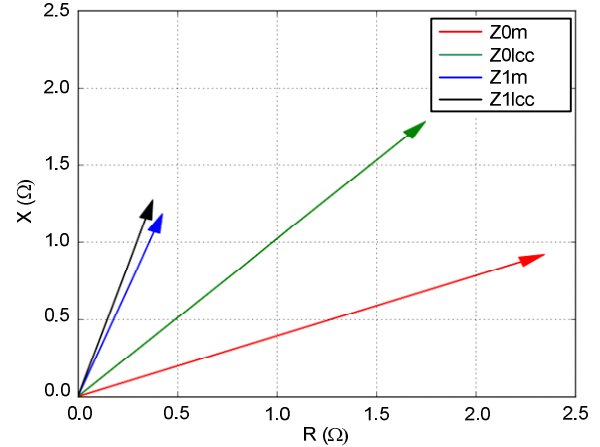


Fig. 23. Measured and computed positive- and zero-sequence impedances for the 5.4-kilometer 115 kV line.

In this case, the difference between the measured and the computed values of the positive- and zero-sequence impedances causes a fault at 80 percent of the line to look like a fault at 88 percent.

We can summarize the previously described results as follows:

- Signal injection is a viable option for utility personnel to measure the line parameters.
- Differences between Z1m and Z1lcc are smaller than the differences between Z0lcc and Z0m.

B. PI Model Approach to Estimate Z1L

Synchrophasor measurements were archived from both ends of a 383-kilometer line during a period of 24 hours. Fig. 24 shows the voltage angle difference between the line ends.

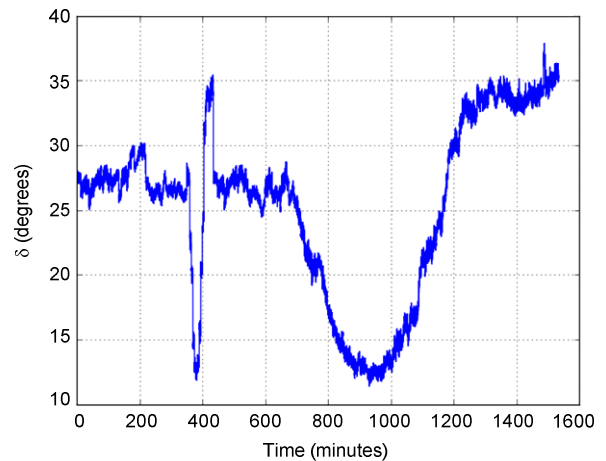


Fig. 24. Positive-sequence voltage angle difference between the ends of the transmission line during a 24-hour period.

Fig. 25 shows the line resistance and reactance calculated using (9) during the 24-hour period.

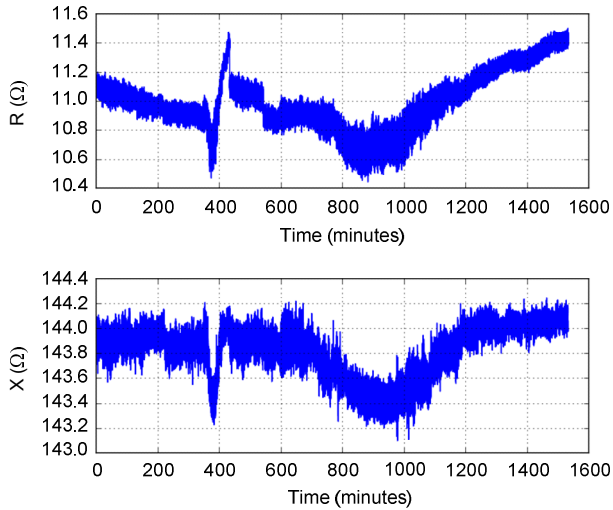


Fig. 25. Estimated line resistance and reactance during a 24-hour period.

The LCC-calculated positive-sequence impedance for this line is $11.6 + j133.4 \Omega$. Averaging the Z1L values obtained during the 24-hour period, the PI model Z1L is $10.99 + j143.8 \Omega$, which is within 10 percent of the LCC calculated value and provides an independent verification of the positive-sequence line impedance.

We classified the estimations in clusters based on the angle difference between the terminals of the line. Fig. 26 shows the impedance variation with respect to the line loading angle. In this case, the top right cluster corresponds to a 35-degree difference. Clusters to the left and down correspond to decreasing angle values, with the cluster at the bottom left corresponding to a 15-degree difference.

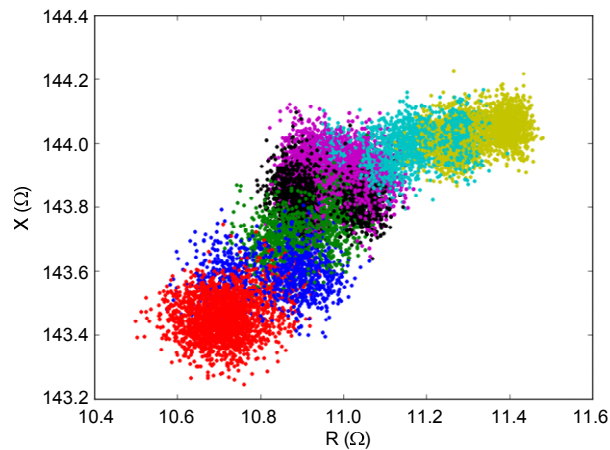


Fig. 26. Line impedance estimation variation with line loading.

C. Line Parameter Calculation Using the SPO Method

Events recorded during a C-phase-to-ground fault (at 242 kilometers from MZD) on a line between MZD and TPD were used to verify the line parameter estimation using the SPO method. Fig. 27 and Fig. 28 show the events captured at the MZD and TPD terminals.

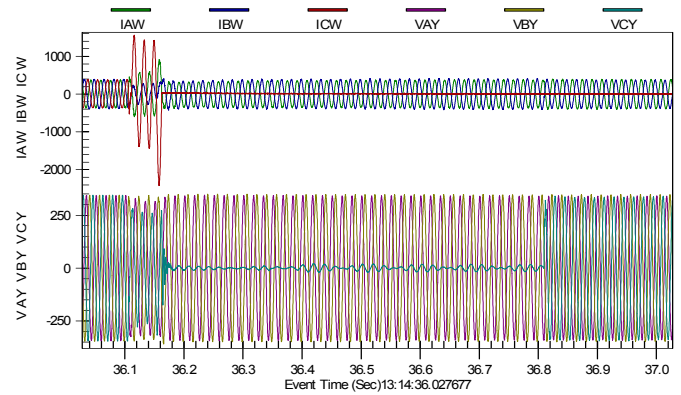


Fig. 27. Event recorded at MZD terminal.

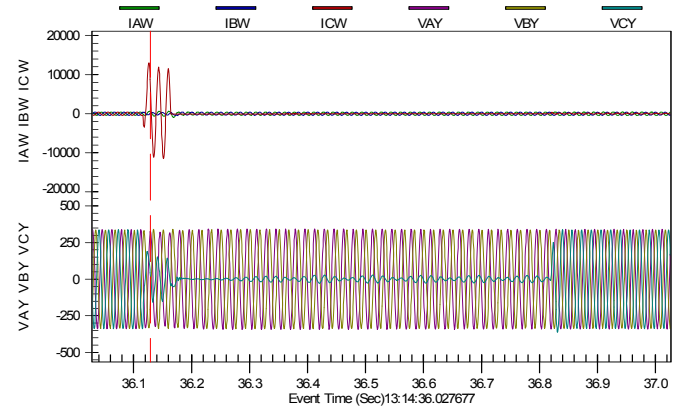


Fig. 28. Event recorded at TPD terminal.

The captured events include the pre-fault load condition, C-phase-to-ground fault, C-phase pole open period, and successful reclose at both terminals. In this event, the TPD terminal recloses 22 cycles before the MZD terminal. CFE uses a sequential reclosing system that monitors the generation at the two line terminals and recloses the terminal with the lowest generation first, which explains the longer reclosing delay at MZD. The data in the SPO window are used to compute the positive- and zero-sequence impedances of the line. Line reactors are in operation at both terminals during this event; therefore, shunt reactor compensation is included in the SPO calculation. Equation (12) shows the provided compensation.

$$I_{p_{\text{compensated}}} = I_p - \frac{V_p}{X_r} \quad (12)$$

where:

I_p is the phase current.

V_p is the phase voltage.

X_r is the reactor impedance.

The compensated currents are used in (10) and (11) to compute the positive- and zero-sequence impedances of the line.

The line impedance is computed for each sample in the SPO data window. Fig. 29 shows the positive-sequence impedance of the line in the impedance plane as calculated by the LCC program and the line impedance estimated using the SPO method.

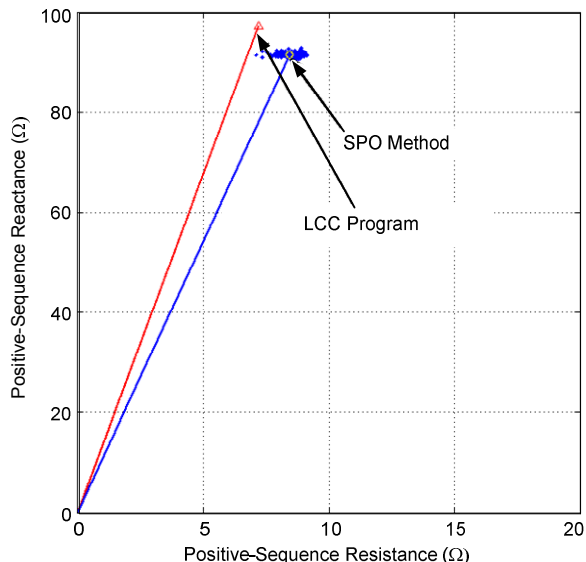


Fig. 29. Positive-sequence line impedance comparison between the LCC and the SPO methods.

Fig. 30 shows the comparison of the zero-sequence line impedance using the SPO method versus the LCC program method.

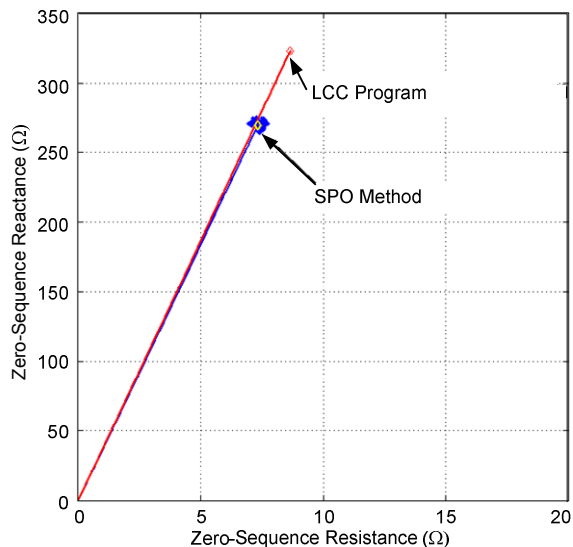


Fig. 30. Zero-sequence line impedance comparison between the LCC and the SPO methods.

Table III shows the values of the estimated line impedances during the SPO condition and the calculated impedances using the LCC program.

TABLE III
ESTIMATED LINE IMPEDANCES WITH THE
LCC PROGRAM AND DURING SPO CONDITIONS

| Method | Positive Sequence (primary ohms) | Zero Sequence (primary ohms) |
|-------------|----------------------------------|------------------------------|
| LCC program | $7.2 + j \cdot 97.32$ | $86.52 + j \cdot 323.4$ |
| SPO | $8.45 + j \cdot 91.66$ | $73.42 + j \cdot 269.45$ |

Fig. 31 shows the correlation of the faulted phase currents at TPD and MZD with the distance element m calculation of the MZD relay during the fault using the LCC and SPO impedance estimates from Table III. Fig. 31 shows that, in this case, the impedance reach setting margins for Zone 1 and Zone 2 accommodate the differences in the m estimates from the LCC and SPO methods.

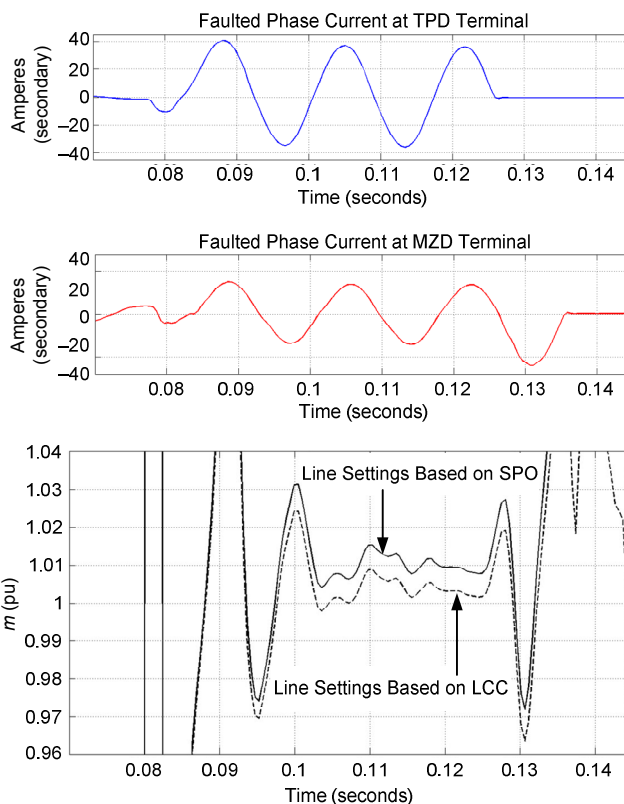


Fig. 31. Calculation of m during the phase-to-ground fault.

VII. FEEDBACK TO DISTANCE AND FAULT LOCATION FUNCTIONS

The event reports from the MZD-TPD line (shown in Fig. 27 and Fig. 28) provide voltages and currents during the fault, during the phase open condition (open poles at both terminals), and when one pole is open at only one terminal (the condition that the proposed SPO method requires).

After the first pole recloses and there is no fault, the relay identifies the desired SPO condition, verifies line loading, calculates the line sequence impedances, and compares them with the relay impedance settings. If the difference is greater than a preestablished threshold, the relay asserts an alarm.

Referring to the MZD-TPD line, we have analyzed only one event that shows differences of 6 percent in Z_{1L} and 16 percent in Z_{0L} , which translates to a difference of less than 2 percent in the m calculation (see Fig. 31). We will analyze more events for faults at other locations and continue monitoring the estimations of Z_{1L} and Z_{0L} before changing the impedance settings.

For the event that we analyzed, the margins of the present relay settings accommodate the existing line parameter, instrument transformer, and relay errors.

VIII. CONCLUSION

Relay engineers calculate transmission line positive- and zero-sequence impedances that are needed to set the relay distance and fault location functions using conductor properties, line geometry, and ground resistivity as inputs to line parameter calculation programs.

In some cases, they apply reduced primary voltages at one end of the line while the remote end is connected to ground to measure these impedances and verify the results from the line parameter calculation program. While this approach provides accurate impedance values, it does not consider VT and CT errors and that impedance value measurements are difficult to obtain.

Synchrophasor measurements during normal operating conditions provide information about the positive-sequence impedance but not the zero-sequence impedance.

This paper presents a method to estimate positive- and zero-sequence impedances, including VT and CT errors, without the need for signal injection. This method requires line-side VTs, breakers with single-pole trip/close mechanisms, voltage and current synchronized measurements, a load angle greater than 5 degrees, and an operating condition where one pole is open at one of the terminals while all of the poles at the remote terminal remain closed. We can use this method to verify the line parameters obtained with line parameter calculation programs and signal injection methods.

Relays can detect single-pole open conditions, perform impedance estimations, and provide alarms when the difference between the estimated values and the relay settings is greater than a predetermined threshold.

IX. APPENDIX

The power system model in Fig. 32 (including the shown positive- and zero-sequence secondary impedance values) was used to analyze the effect of errors in line impedances on the performance of mho distance element and fault location functions in line relays.

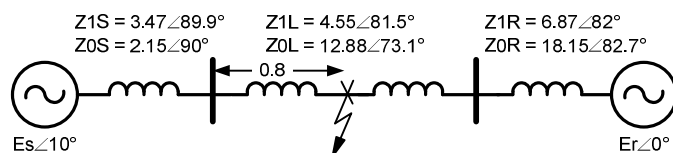


Fig. 32. Two-source power system model.

Voltages and currents at both terminals of the line were computed for an A-phase-to-ground fault with zero fault resistance at 80 percent of the line. Table IV shows the secondary phase voltages and currents during this fault condition.

TABLE IV
FAULT VOLTAGES AND CURRENTS FOR A FAULT
AT 80 PERCENT FROM THE SENDING END

| Voltages and Currents | Sending End | Receiving End |
|-----------------------|-----------------|-----------------|
| A-Phase Voltage | 44.91∠4.81 V | 8.02∠-4.59 V |
| B-Phase Voltage | 65.68∠-110.64 V | 74.11∠-126.34 V |
| C-Phase Voltage | 65.29∠126.17 V | 76.33∠134.15 V |
| A-Phase Current | 7.4∠-69.93 A | 5.81∠-82.95 A |
| B-Phase Current | 1.13∠-88.76 A | 1.13∠91.23 A |
| C-Phase Current | 0.31∠141.44 A | 0.31∠-38.56 A |

X. ACKNOWLEDGMENT

The authors would like to thank Mr. Raj Suyambu for verifying the proposed method to estimate line parameters.

XI. REFERENCES

- [1] M. Grobler and R. Naidoo, "Determining Transmission Line Parameters From GPS Time-Stamped Data," proceedings of the 32nd Annual Conference on IEEE Industrial Electronics, Paris, France, November 2006.
- [2] D. Shi, D. J. Tylavsky, N. Logic, and K. M. Koellner, "Identification of Short Transmission-Line Parameters From Synchrophasor Measurements," proceedings of the 40th North American Power Symposium, Calgary, Canada, September 2008.
- [3] B. Kaszenny, B. Le, and N. Fischer, "A New Multiterminal Fault Location Algorithm Embedded in Line Current Differential Relays," proceedings of the 11th International Conference on Developments in Power System Protection, Birmingham, UK, April 2012.
- [4] D. A. Tziouvaras, J. Roberts, and G. Benmouyal, "New Multi-Ended Fault Location Design for Two- or Three-Terminal Lines," proceedings of the 7th International Conference on Developments in Power System Protection, Amsterdam, Netherlands, April 2001.
- [5] Y. Gong, M. Mynam, A. Guzmán, G. Benmouyal, and B. Shulim, "Automated Fault Location System for Nonhomogeneous Transmission Networks," proceedings of the 65th Annual Conference for Protective Relay Engineers, College Station, TX, April 2012.
- [6] P. M. Anderson, *Power System Protection*. IEEE Press, New York, NY, 1999.
- [7] A. Amberg, A. Rangel, and G. Smelich, "Validating Transmission Line Impedances Using Known Event Data," proceedings of the 65th Annual Conference for Protective Relay Engineers, College Station, TX, April 2012.
- [8] R. Luxenburger and W. de Villiers, "Calculation and Verification of Distance Protection Settings Based on Line Impedance Measurements," proceedings of the 4th Annual Protection, Automation and Control World Conference, Dublin, Ireland, June 2013.
- [9] R. Abboud, W. F. Soares, and F. Goldman, "Challenges and Solutions in the Protection of a Long Line in the Furnas System," proceedings of the 32nd Annual Western Protective Relay Conference, Spokane, WA, October 2005.
- [10] F. Calero and D. Hou, "Practical Considerations for Single-Pole-Trip Line-Protection Schemes," proceedings of the 31st Annual Western Protective Relay Conference, Spokane, WA, October 2004.

- [11] V. H. Serna Reyna, J. C. Rivera Velázquez, H. E. Prado Félix, H. J. Altuve Ferrer, D. Sánchez Escobedo, and J. Gallegos Guerrero, "Transmission Line Single-Pole Tripping: Field Experience in the Western Transmission Area of Mexico," proceedings of the 37th Annual Western Protective Relay Conference, Spokane, WA, October 2010.
- [12] A. Guzmán, V. Mynam, and G. Zweigle, "Backup Transmission Line Protection for Ground Faults and Power Swing Detection Using Synchrophasors," proceedings of the 34th Annual Western Protective Relay Conference, Spokane, WA, October 2007.

XII. BIOGRAPHIES

Hugo E. Prado-Félix received his BSEE in 1982 from the National Polytechnic Institute, Mexico. In 1983, he joined Comisión Federal de Electricidad (CFE), where he was a transmission inspector of the Colima Transmission Subarea from 1983 to 1985 and the Michoacán Transmission Subarea from 1985 to 1987. He was also head of the Protection Office of the Nayarit Transmission Subarea from 1987 to 2002 and head of the Jalisco Transmission Subarea from 2002 to 2005. From 2005 until 2007, he was head of the Protection Department of the Jalisco Transmission Subarea. Since 2007, he has worked as head of the Protection and Metering Office of the CFE Western Transmission Area, where he supervises the installation and commissioning of protection, control, and metering panels.

Víctor H. Serna-Reyna received his BS in mechanical and electrical engineering in 1992 and an MSc in electrical engineering in 1997 from the University of Guadalajara, Mexico. In 1997, he joined Comisión Federal de Electricidad (CFE). Since 2007, he has worked as head of the Studies Department of the CFE Western Transmission Area. His areas of interest are power system analysis and protection.

Mangapathirao V. Mynam received his MSEE from the University of Idaho in 2003 and his BE in electrical and electronics engineering from Andhra University College of Engineering, India, in 2000. He joined Schweitzer Engineering Laboratories, Inc. (SEL) in 2003 as an associate protection engineer in the engineering services division. He is presently working as a senior research engineer in SEL research and development. He was selected to participate in the U.S. National Academy of Engineering (NAE) 15th Annual U.S. Frontiers of Engineering Symposium. He is a senior member of IEEE.

Marcos Donolo received his BSEE from Universidad Nacional de Río Cuarto, Argentina, in 2000, and his masters degree in electrical engineering (2002), his masters degree in mathematics (2005), and his Ph.D. in electrical engineering (2006) from the Virginia Polytechnic Institute and State University. Since 2006, he has been with Schweitzer Engineering Laboratories, Inc., where he is presently a lead research engineer. He is a senior member of IEEE.

Armando Guzmán received his BSEE with honors from Guadalajara Autonomous University (UAG), Mexico. He received a diploma in fiber-optics engineering from Monterrey Institute of Technology and Advanced Studies (ITESM), Mexico, and his MSEE from the University of Idaho, USA. He served as regional supervisor of the Protection Department in the Western Transmission Region of the Federal Electricity Commission (the Mexican electrical utility company) in Guadalajara, Mexico, for 13 years. He lectured at UAG and the University of Idaho in power system protection and power system stability. Since 1993, he has been with Schweitzer Engineering Laboratories, Inc., in Pullman, Washington, where he is a fellow research engineer. He holds numerous patents in power system protection and metering. He is a senior member of IEEE.